Modeling Hysteresis in Pleated Pneumatic Artificial Muscles

M. Van Damme, P. Beyl, B. Vanderborght, R. Van Ham, I. Vanderniepen, R. Versluys, F. Daerden, D. Lefeber
Robotics & Multibody Mechanics Research Group
Vrije Universiteit Brussel, Brussels, Belgium
michael.vandamme@vub.ac.be

***Abstract*—Estimating the force exerted by a pneumatic muscle actuator by measuring its gauge pressure is challenging since hysteresis is almost always present. This paper investigates the hysteresis phenomenon in Pleated Pneumatic Artificial Muscles, which is found to be largely independent of gauge pressure. A Preisach based hysteresis model that can cope with the specific shape of the force-contraction characteristic of pneumatic muscles is proposed, and its results are presented.**

I. Introduction

Pneumatic Artificial Muscles are air-powered contractile actuators that generate linear motion. Their core element is a reinforced membrane that contracts axially and expands radially when pressurized. They have been studied extensively (see [1], [2], [3], [4], [5] and the references therein), and several types have been developed. The most commonly known type is the McKibben muscle [1], [2], a braided muscle that is commercially available from several manufacturers, but other types and variants exist as well (see for instance [6], [7], [8]).

In general, pneumatic artificial muscles are lightweight as well as intrinsically compliant or "soft", because of air compressibility. The increased safety that results from these properties, combined with the trend towards more human-centered robotics and safe human-robot interaction [9], [10], [11], has generated renewed interest in artificial muscle actuation (see for instance [12], [13], [14]). Pneumatic artificial muscles have mainly been applied in rehabilitation (e.g. [15], [16], [17], [14]), but they have also been used in various other fields such as legged machines [18], [19] and even in parachute soft-landing and guidance systems [20].

The artificial muscles used in this work, called Pleated Pneumatic Artificial Muscles, are described in [6], [21], [22]. They have been applied in the bipedal walking robot Lucy [23] and in a "soft" robotic arm [24], [25]. The pleated pneumatic artificial muscle or PPAM was developed to improve on some of the shortcomings of McKibben muscles. It has virtually no threshold pressure, less hysteresis, and it generates higher forces and has a greater contraction range than McKibben muscles.

Since almost all pneumatic muscle based systems use some form of feedback pressure control, these systems are always equipped with pressure sensors. Theoretically, the measured pressure could be used to estimate the force exerted by the actuator. In reality, however, hysteresis is always present, which can make the estimates too inaccurate to be useful. In this work, we present a first step towards the solution of this problem in the case of the PPAM muscle.

This work is supported by the Fund for Scientific Research (FWO) - Flanders (Belgium) and by the Research Council (OZR) of the Vrije Universiteit Brussel.

Figure 1. A Pleated Pneumatic Artificial Muscle (PPAM) shown for three different values of contraction.

This paper is organized as follows: section II introduces the PPAM muscle and its theoretical model, section III discusses the hysteresis phenomenon in the muscle, proposes a Preisach-based hysteresis model and presents some results obtained with this model. Conclusions are drawn in section IV.

II. Pleated Pneumatic Artificial Muscles

A. Concept

Pneumatic artificial muscles (PAMs) are contractile devices whose core element is an inflatable membrane. When inflated they bulge, shorten and thereby generate a contraction force. The most common type, the McKibben muscle [1], [2], consists of a rubber tube, which expands when inflated, surrounded by a netting that transfers tension. Although relatively easy to make, the McKibben muscle has some important drawbacks, such as substantial hysteresis and a high threshold pressure, under which no contraction occurs. Its total displacement is limited to just 20% to 30% of the initial length. To remedy these problems, a new type of PAM has been developed, the PPAM [6], [21], [22]. The PPAM (see figure 1) has a folded membrane that unfolds as it expands. Force is transferred by Kevlar fibres in the pleats of the membrane. Because of the unfolding, there is virtually no threshold pressure, hysteresis is reduced when compared to McKibben muscles, and contractions of over 40% are possible (depending on the slenderness, described in the next section).

978–1–4244–1676–9/08/$25.00 © 2008 IEEE

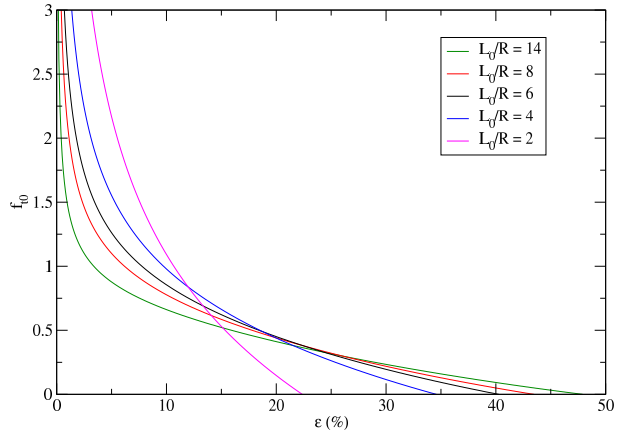

Figure 2. f_{t0} (dimensionless force function) of a PPAM with $N = 25$ Kevlar fibres.

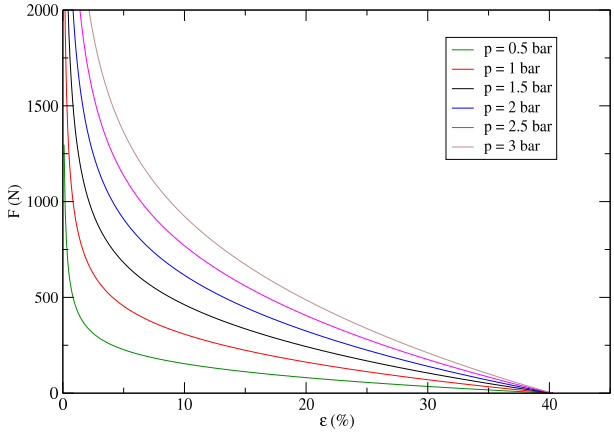

Figure 3. Force exerted by a PPAM with $l_0/R = 6$, $l_0 = 6$ cm and $N = 25$ for different gauge pressures.

B. *Characteristics*

A relatively accurate mathematical model that describes shape, volume, diameter, exerted force and maximum contraction of PPAMs can be found in [22], [6], [26]. Under the assumption of negligible membrane elasticity the static force exerted by the muscle is given by

$$F = pl_0^2 f_{t0}\left(\epsilon, l_0/R, N\right) \tag{1}$$

In this expression, p is the applied gauge pressure, l_0 is the muscle's uncontracted length (or maximum length), R is its radius in uncontracted state (or minimum radius), N is the number of Kevlar fibres in the muscle and ϵ is the muscle contraction. If we call l the muscle length, we have $\epsilon = 1 - l/l_0$. f_{t0} is a nonlinear, dimensionless function that depends on contraction and on the design-time parameter l_0/R (called the slenderness). f_{t0} is shown in figure 2 for different values of l_0/R. As figure 2 and equation (1) show, there is a varying force-displacement relation at constant gauge pressure. This results in muscle-like behaviour, with very high forces being generated at small contractions and very low forces at large contractions, as shown in figure 3 for a muscle with slenderness $l_0/R = 6$ and $l_0 = 6$ cm. Due to the inelastic approximation used in deriving (1), this model is only valid for contractions above 5% [26]. This is not a problem since the contraction should generally be kept above 5% anyway, to avoid excessive material loading.

In practice, the dimensionless function $f_{t0}\left(\epsilon, l_0/R, N\right)$ is difficult to work with since it is not available in analytical form. In order to evaluate it for given ϵ and l_0/R, a system of equations involving elliptic integrals has to be solved numerically (see [26], [6]). Another problem is that the radius R is usually not accurately known, and varies slightly between different muscles. For these reasons, the full mathematical model is usually only used during the design phase of a system that involves PPAMs. Once the slenderness and number of fibres is known, f_{t0} is approximated by a function of the following form [22]:

$$f_{t0}\left(\epsilon\right) \approx f_0\epsilon^{-1} + f_1 + f_2\epsilon + f_3\epsilon^2 + f_4\epsilon^3. \tag{2}$$

The coefficients are determined by fitting (2) to the theoretical f_{t0} or to measured data.

III. Hysteresis in PPAMs

Chou and Hannaford [2] report that the main cause for hysteresis in the McKibben muscle is Coulomb friction between the braided mesh shell and the internal bladder. Although the PPAM has a different working principle, it too displays hysteresis in the force-contraction characteristic, but less than the McKibben muscle. This hysteresis is not modeled in (1).

A. *Experiments*

Fig. 4 shows the experimentally obtained force-contraction characteristic of a PPAM with 40 fibres. These measurements have been performed with the muscle mounted in a tensile testing machine and the following sinusoidal force function imposed:

$$F(t) = A\sin\left(\omega t\right) + B,$$

with $A = 1400\,N$, $B = 750\,N$ and $\omega = 2\pi/500\,\mathrm{rad}/s$. The gauge pressure was controlled to be as constant as possible by a pneumatic servo valve. One period is shown for each gauge pressure. The hysteresis is clearly visible.

Fig. 5 shows the dimensionless force function f_{t0}, obtained from the same data by computing the quantities $F_m\left(t\right)/p_m\left(t\right)l_0^2$ (see eq. (1)), and plotting them against $\epsilon_m\left(t\right)$. In these expressions, $F_m\left(t\right)$ is the measured force at time t, $p_m\left(t\right)$ the measured pressure and $\epsilon_m\left(t\right)$ the measured contraction.

For contractions above $5\,\%$, the hysteresis observed in the dimensionless force function f_{t0} does not differ significantly between the three curves shown (the difference for contractions below 5% can be explained by the elastic behaviour of the muscle fibres, which is not taken into account in (1)). This indicates that the hysteresis in f_{t0} is essentially pressure independent.

Fig. 6 shows the measured dimensionless force function of a PPAM with 25 fibres. These measurements were taken while the muscle was fitted in a 2-DOF arm powered by PPAMs

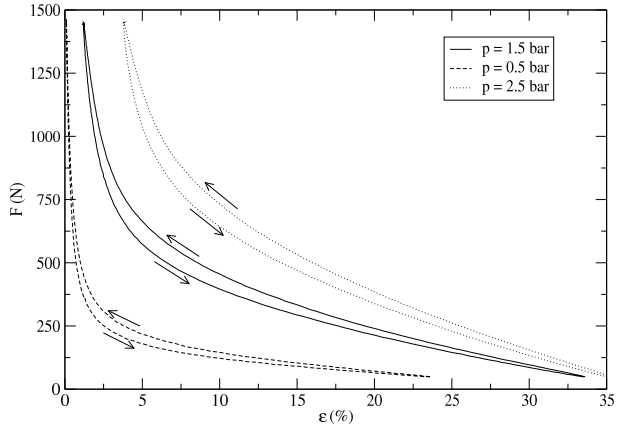

Figure 4. Measured force-contraction curves of a PPAM with $l_0/R \approx 6$, $l_0 = 6$ cm and $N = 40$ fibres for different gauge pressures.

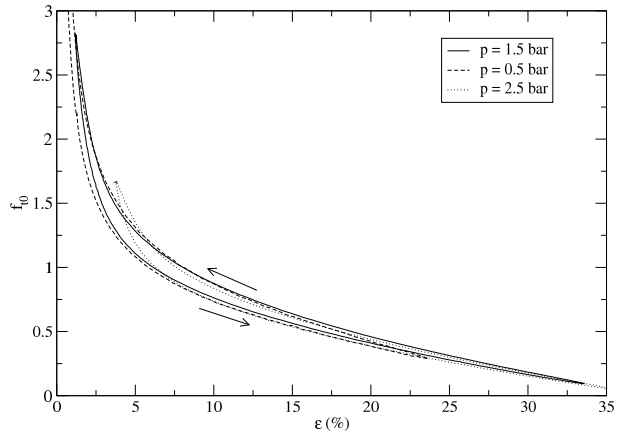

Figure 5. Measured dimensionless force function of a PPAM with $l_0/R \approx 6$, $l_0 = 6$ cm and $N = 40$ fibres for different gauge pressures.

(see fig. 7, more information can be found in [24]). While the gauge pressure was kept as constant as possible by a servo valve, the link powered by the muscle was rotated manually, and the muscle force and contraction were measured. For easy comparison, a curve from figure 5 (taken from a muscle with 40 fibres) is also shown in fig. 6.

Once again the different curves do not differ significantly, indicating independence of gauge pressure. The fact that the dimensionless force function for $N = 25$ is lower than for $N = 40$ is consistent with the theoretical model [22]. It is striking, however, that the hysteresis effect is much less pronounced for the case $N = 25$ than for the case $N = 40$. This indicates that friction between the Kevlar fibres and the membrane may be an important contributing factor to the hysteresis.

Since the link rotation in the experiment was performed manually, it was impossible to achieve a constant contraction rate. Fig. 8 shows two measurements (with $N = 25$), one where the link was moved relatively slowly (roughly 40 seconds for the loop shown) and a second one where it was moved five times faster (around 8 seconds for the loop in the figure). The two curves hardly differ. Since the same kind of experiment but with different gauge pressures yields the same

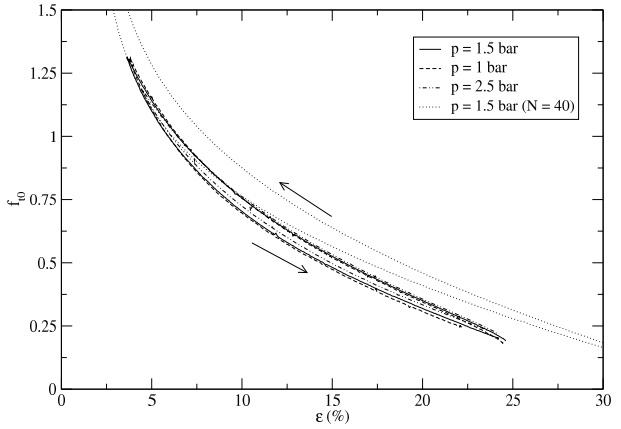

Figure 6. Measured dimensionless force function of a PPAM with $l_0/R \approx 6$, $l_0 = 6$ cm and $N = 25$ fibres for different gauge pressures. For reference, one curve measured for a similar muscle with $N = 40$ is also shown.

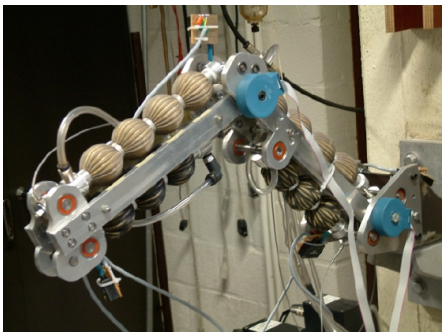

Figure 7. 2-DOF robotic arm powered by Pleated Pneumatic Artificial Muscles.

result, the hysteresis in f_{t0} seems to be independent of the contraction rate.

B. Modeling

The experiments suggest that the hysteresis in PPAMs can by modeled by incorporating hysteresis into the dimensionless force function f_{t0}. Since most phenomenological hysteresis

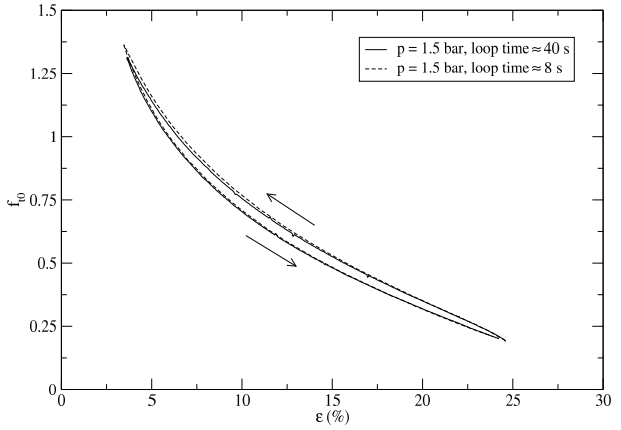

Figure 8. Measured dimensionless force function of a PPAM with $l_0/R \approx 6$, $l_0 = 6$ cm and $N = 25$ fibres for different loop speeds.

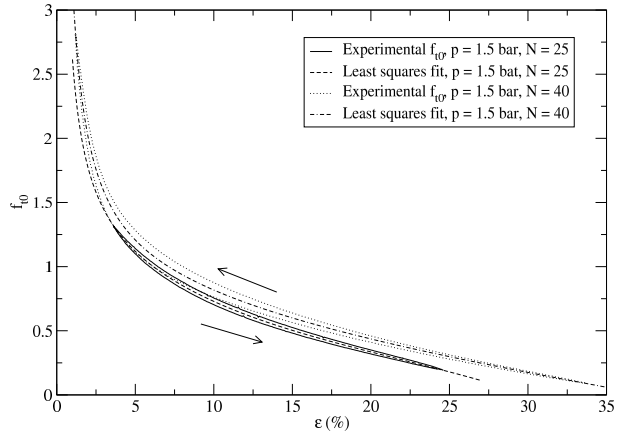

Figure 9. Measured and approximated dimensionless force function of PPAMs with 25 and 40 fibres. Both have $l_0/R \approx 6$ and $l_0 = 6$ cm.

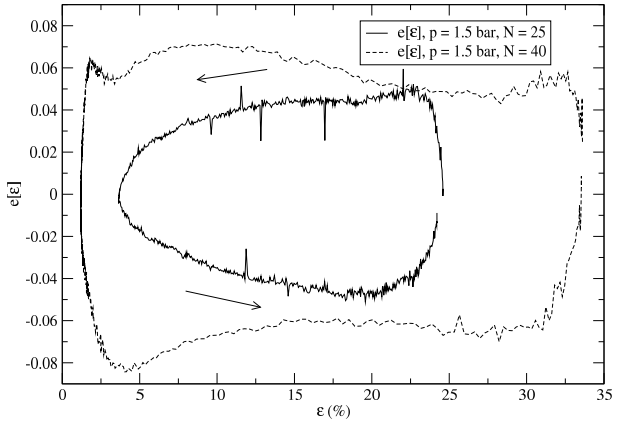

Figure 10. Relative error $e[\epsilon]$ between the measured and approximated dimensionless force function of PPAMs with 25 and 40 fibres. Both have $l_0/R \approx 6$ and $l_0 = 6$ cm.

models have difficulties describing hysteresis loops whose general form resembles that of f_{t0} (see fig. 2), we cannot model the hysteresis in f_{t0} directly.

This can be overcome by looking at the error between the observed (hysteretic) f_{t0}^{hyst} and its least-squares fit f_{t0}^{fit} of the form (2). Modelling the hysteretic muscle force as (cf. eq. (1))

$$\begin{aligned} F^{\text{hyst}} &= p l_0^2 f_{t0}^{\text{hyst}}[\epsilon] \\ &= p l_0^2 f_{t0}^{\text{fit}}(\epsilon) \cdot (1 + e[\epsilon]) \end{aligned} \tag{3}$$

we get

$$e[\epsilon] = \frac{f_{t0}^{\text{hyst}}[\epsilon]}{f_{t0}^{\text{fit}}(\epsilon)} - 1, \tag{4}$$

the relative error between the observed hysteretic dimensionless force function and its least-squares fit. In these equations, square brackets have been used to indicate quantities that depend hysteretically on ϵ, i.e. that depend on the current value of ϵ as well as on certain past values. Fig. 9 shows the measured f_{t0} for both muscles ($N = 40$ and $N = 25$, both measured at $p = 1.5$ bar), as well as their fitted approximations, and fig. 10 shows the relative error $e[\epsilon]$ for both cases.

The relative error $e[\epsilon]$ between the hysteretic curve and its approximation is no longer dependent on the specific shape of the dimensionless force function, which has been factored out (see $f_{t0}^{\text{fit}}(\epsilon)$ in (3)). This means we can model $e[\epsilon]$ by taking the scaled difference between a more conventional hysteretic loop (one that can easily be generated by a hysteresis model) and its non-hysteretic linear approximation (see fig. 11). It is clear that we cannot expect a perfect match, since the exact shape of $e[\epsilon]$ is not fully reproducible among experiments.

C. The Preisach Model

The exact hysteresis model used is not crucial to our approach, as long as the output of the model always stays inside the major loop. Since it is well studied [27], intuitive, invertible under mild conditions (see e.g. [28], [29]), and because it has already been applied to various problems outside of its original scope (see for instance [30], [31], [32]), we have

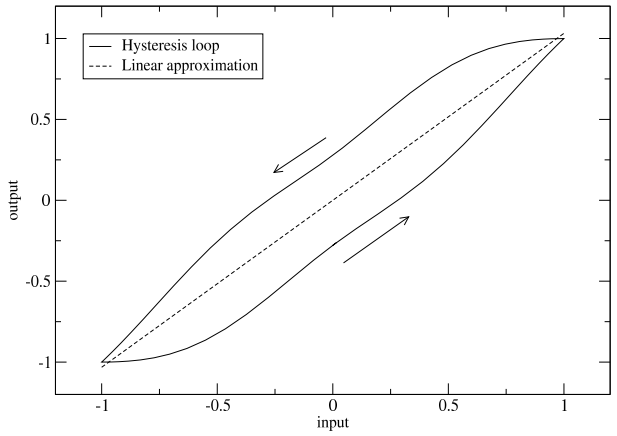

Figure 11. Major hysteresis loop calculated with the Preisach model, and its linear approximation.

chosen for the Preisach model. It was Introduced in the 1930's by F. Preisach to model magnetic hysteresis [33], and has been called the most satisfactory mathematical model of hysteresis available [28].

The output of the Preisach model is calculated as the weighted superposition of elementary relay hystereses $\gamma_{\alpha\beta}[u]$ (see fig. 12). Each relay has two switching values α and β (with $\alpha > \beta$), so the relays can be represented by points in the half-plane $\alpha > \beta$. The contribution of each relay to the output of the Preisach model is determined by a weighing function μ:

$$W[u] = \int\int_P \mu(\alpha, \beta) \cdot \gamma_{\alpha\beta}[u] \, d\alpha d\beta.$$

The region P of support of $\mu(\alpha, \beta)$ in the half-plane $\alpha > \beta$ is usually referred to as the Preisach plane. In this work, we will assume this region to be bound between the lines $\beta = -1$, $\beta = 1$ and $\alpha = 1$, as shown in fig. 13. We will also assume that $\mu(\alpha, \beta)$ is normalized in P, i.e. $\int\int_P \mu(\alpha, \beta) \, d\alpha d\beta = 1$. P is divided in two parts, P_+ and P_-, in which the relays $\gamma_{\alpha\beta}$ have outputs $+1$ and -1 respectively, so we have

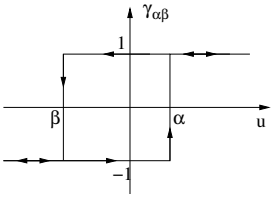

Figure 12. Elementary relay $\gamma_{\alpha\beta}[u]$

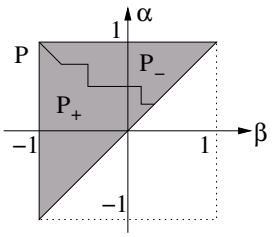

Figure 13. Preisach plane P (in gray), divided in P_+ (relays with output $+1$) and P_- (relays with output -1) by the typical staircase line.

$$W[u] = \int\int_{P_+} \mu(\alpha,\beta)\, d\alpha d\beta - \int\int_{P_-} \mu(\alpha,\beta)\, d\alpha d\beta.$$

The boundary between P_+ and P_- is a staircase line, as explained in for instance [27], [32]. The "memory" of the Preisach model is encoded in the shape of this line.

The major hysteresis loop shown in fig. 11 is the output of the Preisach model to one period of a sine function as input and with the normalization $\tilde{\mu}(\alpha,\beta)$ of

$$\mu(\alpha,\beta) = \begin{cases} e^{-(\beta-\alpha-c)^2-(\beta+\alpha-d)^2} & \alpha+\beta \le 0 \\ e^{-(\beta-\alpha-c)^2-(\beta+\alpha+d)^2} & \alpha+\beta > 0 \end{cases} \quad (5)$$

as weight function, where $c = -0.1$ and $d = -1$ [34].

D. Application to the PPAM

Using the above described Preisach model, we now write $e[\epsilon]$ form eq. (3) as

$$e[\epsilon] = \delta \cdot \left(W[\epsilon_s] - W^{\text{fit}}(\epsilon_s) \right),$$

with

$$-1 \le \epsilon_s = 2\frac{\epsilon}{\epsilon\text{max}} - 1 \le 1. \quad (6)$$

δ is a scaling factor. $W[\epsilon_s]$ is the output of the Preisach model and $W^{\text{fit}}(\epsilon_s)$ is the linear approximation obtained by fitting the two major loops generated by $W[\epsilon_s]$. Both $W[\epsilon_s]$ and $W^{\text{fit}}(\epsilon_s)$ are shown in fig. 11 for weight function $\tilde{\mu}$ (see (5)).

Definition (6) of ϵ_s assumes the major hysteresis loop of f_{t0} to be between $\epsilon = 0$ and $\epsilon = \epsilon\text{max}$, which are mapped to -1 and 1 respectively, the minimum and maximum input values of the considered Preisach model. In what follows, the value of ϵmax was chosen to be 35%.

The hysteresis model of the PPAM muscle thus becomes

$$\begin{aligned} F^{\text{hyst}} &= p l_0^2 f_{t0}^{\text{hyst}}[\epsilon] \\ &= p l_0^2 f_{t0}^{\text{fit}}(\epsilon) \cdot \left(1 + \delta \cdot \left(W[\epsilon_s] - W^{\text{fit}}(\epsilon_s) \right)\right) \end{aligned} \quad (7)$$

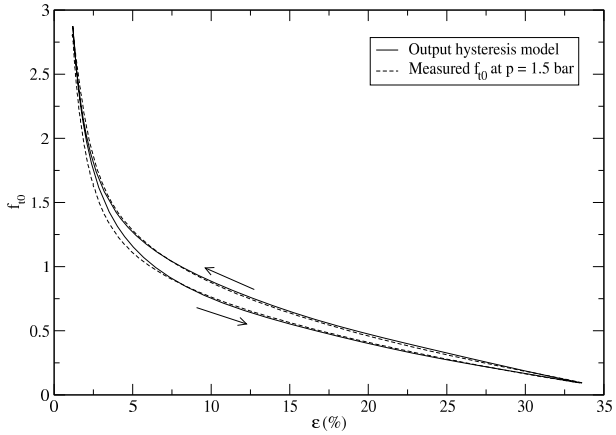

Figure 14. The dimensionless force function $f_{t0}^{\text{hyst}}[\epsilon]$ as calculated by the hysteresis model. The experimentally determined values for $p = 1.5$ bar are also shown. Muscle parameters were $l_0/R \approx 6$, $l_0 = 6$ cm and $N = 40$.

E. Results

Fig. 14 shows the result of the model for the muscle with 40 fibres using $\tilde{\mu}$ (cf. (5)). The fit f_{t0}^{fit} was obtained from the measurements taken at $p = 1.5$ bar (also shown in the figure), and the optimal value of δ was determined with the least-squares method ($\delta \approx 0.299$). The correspondence between model and measurement is good for $7\% \le \epsilon \le 20\%$, the most important region in applications. This result is slightly misleading, however, since the muscle isn't usually used at constant pressure.

In the following test (performed with data taken from the muscle with 25 fibres), we started out the same way: f_{t0} was fitted from the data taken at 1.5 bar, and an optimal value for δ was estimated from this data ($\delta \approx 0.139$). Next, f_{t0}^{fit} was calculated again, this time from all available data (taken at gauge pressures of 1 bar, 1.5 bar and 2.5 bar), while δ wasn't changed. Finally, the muscle's output force was calculated from the hysteresis model (7) for the three cases. The result is shown in fig. 15. Again, the most important deviations are situated in the low ϵ ranges. This is due to inaccuracies both in the model and in f_{t0}^{fit}, which isn't perfectly tuned for all gauge pressures. It is important to remark that the forces shown in fig. 15 were calculated using measured pressure values, the pressures were not assumed to be exactly equal to their desired values. Slight pressure deviations (which always occur because of disturbances and imperfections in the pressure regulating valves) can generate considerable force differences in PPAMs, so they have to be taken into account.

IV. Conclusions and Future Work

The hysteresis phenomenon in PPAM muscles was experimentally investigated. It was found that the hysteresis in the dimensionless force function f_{t0} is largely independent of gauge pressure and contraction rate. The main physical cause of the hysteresis seems to be friction between the Kevlar fibres and the inflatable membrane.

A Preisach-based model for the hysteresis was proposed, and its results were presented. The model performs well for

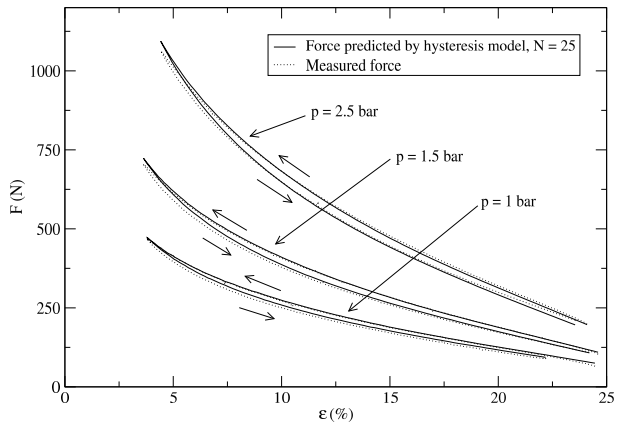

Figure 15. Muscle force as calculated by the hysteresis model, as well as measured values. Muscle parameters were $l_0/R \approx 6$, $l_0 = 6$ cm and $N = 25$.

the contraction range that is most important in applications, i.e. $7\% \leq \epsilon \leq 20\%$.

Future work will focus on numerically determining a better Preisach weight function μ from experimental data in order to further expand the contraction range where there is good agreement between the model and the experiments.

REFERENCES

[1] H. F. Schulte, "The characteristics of the McKibben artificial muscle," in *The Application of External Power in Prosthetics and Orthotics*, no. Publication 874, pp. 94–115, National Academy of Sciences - National Research Council, Washington DC, 1961.

[2] C. P. Chou and B. Hannaford, "Measurement and modelling of McKibben Pneumatic Artificial Muscles," *IEEE Transactions on Robotics and Automation*, vol. 12, no. 1, pp. 90–102, 1996.

[3] G. K. Klute, J. M. Czerniecki, and B. Hannaford, "Artificial Muscles: Actuators for Biorobotic Systems," *The International Journal of Robotics Research*, vol. 21, no. 4, pp. 295–309, 2002.

[4] B. Tondu and P. Lopez, "Modeling and Control of McKibben Artificial Muscle Robot Actuators," *IEEE Control Systems Magazine*, vol. 20, no. 2, pp. 15–38, 2000.

[5] D. W. Repperger, C. A. Philips, D. C. Johnson, R. D. Harmon, and K. Johnson, "A Study of Pneumatic Muscle Technology for Possible Assistance in Mobility," in *Proceedings of the 19th Annual International Conference of the IEEE Engineering in Medicine and Biology society*, vol. 5, pp. 1884–1887, 1997.

[6] F. Daerden and D. Lefeber, "The concept and design of pleated pneumatic artificial muscles," *International Journal of Fluid Power*, vol. 2, no. 3, pp. 41–50, 2001.

[7] W. Liu and C. R. Rahn, "Fiber-Reinforced Membrane Models of McKibben Actuators," *Transactions of the ASME - E - Journal of Applied Mechanics*, vol. 70, no. 6, pp. 853–859, 2003.

[8] N. Saga, T. Nakamura, and K. Yaegashi, "Mathematical Model of Pneumatic Artificial Muscle Reinforced by Straight Fibers," *Journal of Intelligent Material Systems and Structures*, vol. 18, pp. 175–180, Feb. 2007.

[9] A. Bicchi and G. Tonietti, "Fast and soft arm tactics: Dealing with the safety-performance trade-off in robot arms design and control," *IEEE Robotics and Automation Magazine*, vol. 11, no. 2, pp. 22–33, 2004.

[10] M. Zinn, B. Roth, Khatib O., and J. K. Salisbury, "A New Actuation Approach for Human Friendly Robot Design," *The International Journal of Robotics Research*, vol. 23, no. 4-5, pp. 379–398, 2004.

[11] D. Kulic and E. A. Croft, "Real-time safety for human-robot interaction," *Robotics and Autonomous Systems*, vol. 54, no. 1, pp. 1–12, 2006.

[12] J. Surentu, J. M. G. Tuijthof, and J. L. Herder, "Optimized artificial muscles for an inherently safe robotic arm," in *Proceedings of the 2007 IEEE 10th International Conference on Rehabilitation Robotics*, pp. 1070–1076, June 2007.

[13] S. Balasubramanian, J. Ward, T. Sugar, and J. He, "Characterization of the Dynamic Properties of Pneumatic Muscle Actuators," in *Proceedings of the 2007 IEEE 10th International Conference on Rehabilitation Robotics*, pp. 764–770, June 2007.

[14] K. E. Gordon, G. S. Sawickia, and D. P. Ferris, "Mechanical performance of artificial pneumatic muscles to power an anklefoot orthosis," *Journal of Biomechanics*, vol. 39, pp. 1832–1841, 2006.

[15] T. Noritsugu and T. Tanaka, "Application of a Rubber Artificial Muscle Manipulator as a Rehabilitation Robot," *IEEE/ASME Transactions on Mechatronics*, vol. 2, no. 4, pp. 259–267, 1997.

[16] N. G. Tsagarakis and G. Caldwell, "Development and Control of a "Soft-Actuated" Exoskeleton for Use in Physiotherapy and Training," *Autonomous Robots*, vol. 15, pp. 21–33, 2003.

[17] B. Tondu, S. Ippolito, J. Guiochet, and A. Daidie, "A Seven-degrees-of freedom Robot-arm Driven by Pneumatic Artificial Muscles for Humanoid Robots," *The International Journal of Robotics Research*, vol. 24, no. 4, pp. 257–274, 2005.

[18] B. Vanderborght, B. Verrelst, R. Van Ham, and D. Lefeber, "Controlling a Bipedal Walking Robot Actuated by Pleated Pneumatic Artificial Muscles," *Robotica*, vol. 24, pp. 401–410, July 2006.

[19] C. S. Tzafestas, N. K. M'Sirdi, and N. Manamani, "Adaptive Impedance Control Applied to a Pneumatic Legged Robot," *Journal of Intelligent and Robotic Systems*, vol. 20, pp. 105–129, 1997.

[20] W. Zhang, M. L. Accorsi, and J. W. Leonard, "Analysis of geometrically nonlinear anisotropic membranes: application to pneumatic muscle actuators," *Finite Elements in Analysis and Design*, vol. 41, pp. 944–962, 2005.

[21] F. Daerden and D. Lefeber, "Pneumatic artificial muscles: actuators for robotics and automation," *European Journal of Mechanical and Environmental Engineering*, vol. 47, no. 1, pp. 10–21, 2002.

[22] B. Verrelst, R. Van Ham, B. Vanderborght, D. Lefeber, F. Daerden, and M. Van Damme, "Second generation pleated pneumatic artificial muscle and its robotic applications," *Advanced Robotics*, vol. 20, no. 7, pp. 783–805, 2006.

[23] B. Verrelst, R. Van Ham, B. Vanderborght, F. Daerden, and D. Lefeber, "The Pneumatic Biped "LUCY" Actuated with Pleated Pneumatic Artificial Muscles," *Autonomous Robots*, vol. 18, pp. 201–213, 2005.

[24] M. Van Damme, F. Daerden, and D. Lefeber, "A pneumatic manipulator used in direct contact with an operator," in *Proceedings of the 2005 IEEE International Conference on Robotics and Automation*, (Barcelona, Spain), pp. 4505–4510, April 2005.

[25] M. Van Damme, B. Vanderborght, R. Van Ham, B. Verrelst, F. Daerden, and D. Lefeber, "Proxy-Based Sliding Mode Control of a Manipulator Actuated by Pleated Pneumatic Artificial Muscles," in *Proceedings of the 2007 IEEE International Conference on Robotics and Automation (ICRA2007)*, pp. 4355–4360, Apr. 2007.

[26] F. Daerden, *Conception and Realization of Pleated Pneumatic Artificial Muscles and their Use as Compliant Actuation Elements*. PhD thesis, Vrije Universiteit Brussel, 1999.

[27] I. D. Mayergoyz, *Mathematical Models of Hysteresis*. Springer Verlag, New York, 1991.

[28] M. Brokate and A. Visintin, "Properties of the Preisach model for hysteresis," *Journal fur die reine und angewandte Mathematik*, vol. 402, pp. 1–40, 1989.

[29] M. Brokate, "Some Mathematical Properties of the Preisach Model for Hysteresis," *IEEE Transactions on Magnetics*, vol. 25, no. 4, pp. 2922–2924, 1989.

[30] M. Frankowicz and M. Chrenowski, "Application of Preisach model to adsorption-desorption hysteresis," *Physica B*, vol. 372, pp. 219–221, 2006.

[31] H. Hu and R. Ben Mrad, "On the classical Preisach model for hysteresis in piezoceramic actuators," *Mechatronics*, vol. 13, pp. 85–94, 2003.

[32] R. B. Gorbet, *Control of Hysteretic Systems with Preisach Representations*. PhD thesis, University of Waterloo, 1997.

[33] F. Preisach, "Uber die magnetische Nachwirkung," *Zeitschrift fur Physik*, vol. 94, pp. 277–302, 1935.

[34] S. Zsolt, *Hysteresis models from elementary operators and integral equations*. PhD thesis, Budapest University of Technology and Economics, 2002.